Stimulus-Driven Liquid Metal and Liquid Crystal Network Actuators for Programmable Soft Robotics

Received 00th January 20xx,
Accepted 00th January 20xx

DOI: 10.1039/x0xx00000x

www.rsc.org/

Pengfei Lv[a†], Xiao Yang[a†], Hari Krishna Bisoyi[b†], Hao Zeng[c], Xuan Zhang[a], Yuanhao Chen[a], Pan Xue[a], Shukuan Shi[a], Arri Priimagi[c], Ling Wang*[a], Wei Feng*[a,d,e], and Quan Li*[b,f]

Sophisticated soft matter engineering has been endorsed as an emerging paradigm for developing untethered soft robots with built-in electronic functions and biomimetic adaptation capacities. However, the integration of flexible electronic components into soft robotic actuators is challenging due to the strain mismatch and materials incompatibility. Herein, we report a general strategy to integrate electrically conductive liquid metals (LMs) and shape-morphing liquid crystal networks (LCNs) towards multifunctional and programmable soft robotics. A unique colloidal LM ink with superior adhesion and photothermal conversion efficiency was judiciously designed and fabricated by ultrasonicating LMs and miniature carboxylated gold nanorods (MiniGNR-COOH) in an aqueous suspension of biological bacterial cellulose. The designed nanocellulose-based colloidal LM ink is used for shape-deformable and electrically conductive LM-LCN soft robots that can be electro- and photo-thermally actuated. As proof-of-concept demonstrations, we present a light-fueled soft oscillator, inchworm-inspired soft crawler and programmable robotic Shadow Play exhibiting multifunctional controllability. The strategy disclosed here could open up a new technological arena for advanced multifunctional soft materials with potential utility in bioinspired soft machines, integrated soft electronics, human-computer interaction and beyond.

Introduction

Nature has long been a source of inspiration for mimicking the biological softness, body compliance and vital functions of diverse living organisms, perhaps the prime examples being the octopus, adapting to unstructured environments, and the skeletal muscles, generating active force and sophisticated motions.[1-4] Bio-inspired soft-bodied robots engineered from responsive soft materials have recently attracted increasing attention from the perspective of both fundamental discoveries and promising technological applications. They possess several attractive features compared to conventional rigid robots such as structural deformability, human-friendly interaction, high degree of freedom for actuation as well as environmental compliance and adaptability.[5,6] In this context, researchers have devoted extensive efforts to the development of soft robotic actuation strategies with built-in biomimetic intelligence, based on various responsive soft materials such as hydrogels, liquid crystal networks (LCNs) and shape memory polymers (SMPs).[7-13] Thanks to the anisotropic, reversible and programmable shape-morphing properties, LCNs have been considered particularly promising for stimulus-driven soft actuators with diverse robotic motions, such as gripping, walking, swimming and oscillation, and intelligent functions including reconfigurability, self-regulation and associative learning.[14-24] However, LCN-based soft robotic systems are often limited by their inadequate intrinsic thermal or electrical conductivity and mechanical incompatibility with functional nanomaterials.

Gallium-based liquid metals (LMs) are currently in the limelight of soft robotics research owing to their unprecedented merits in terms of superior fluidity, outstanding shape-deformability, high thermal and electrical conductivity, tailorable photothermal characteristics and excellent biocompatibility.[25,26] Nevertheless, shape-transformation and adaptive locomotion of LM-based soft robots are mostly driven by electric field or chemical stimuli, and often in aqueous acidic environment to prevent surface oxidation, which greatly limits their functionality and potential application scenarios. As a result, hybrid systems combining LMs and stimuli-responsive smart materials are recently receiving increasingly important attentions.[27,28] For example, light-driven LM-based shape-transformers were achieved by encapsulating LM microdroplets within graphene-quantum-dot-containing polydopamine, prompting an enhanced photothermal conversion efficiency.[29-31] With LM microdroplets suspended in soft elastomer matrices, stretchable composite films with high dielectric constant, thermal conductivity and electrically self-healing ability, have been reported.[32-35] Also natural cellulose nanofibrils have been applied as structural matrix for LM microdroplets to fabricate conductive and free-standing soft LM actuators responding to humidity and electric field.[36,37] Anisotropic LM-contained liquid crystalline polymer composites have been investigated for electrically-activated shape-morphing soft actuators with coupled sensing capability by embedding LM microdroplets into a compliant liquid crystalline matrix.[38,39] The thermal conductivity of the resulting composites was greatly enhanced, and electrical conductivity could be invoked by mechanical sintering, leading to the formation of oxidation shells around the embedded LM microparticles. Recently, hydrogen-doping by ultrasonication in the presence of aliphatic polymers has been reported to endow the insulating oxide skin around viscoplastic LM microparticles with high electrical conductivity.[40] Although great

[a] School of Materials Science and Engineering, Tianjin University, Tianjin 300350, P. R. China. *E-mail: lwang17@tju.edu.cn (L.W.); weifeng@tju.edu.cn (W.F.)
[b] Advanced Materials and Liquid Crystal Institute and Chemical Physics Interdisciplinary Program, Kent State University, Kent, OH 44242, USA. Smart Photonic Materials, Faculty of Engineering and Natural Sciences, Tampere University, P.O. Box 541, Tampere, FI-33101 Finland
[c] Key Laboratory of Advanced Ceramics and Machining Technology, Ministry of Education, Tianjin 300350, P. R. China.
[d] Key Laboratory of Materials Processing and Mold, Ministry of Education, Zhengzhou University, Zhengzhou, 450002, China.
[e] Institute of Advanced Materials and School of Chemistry and Chemical Engineering, Southeast University, Nanjing 211189, China. *E-mail: quanli3273@gmail.com or qli1@kent.edu (Q. L.)
† These authors contributed equally to this work.

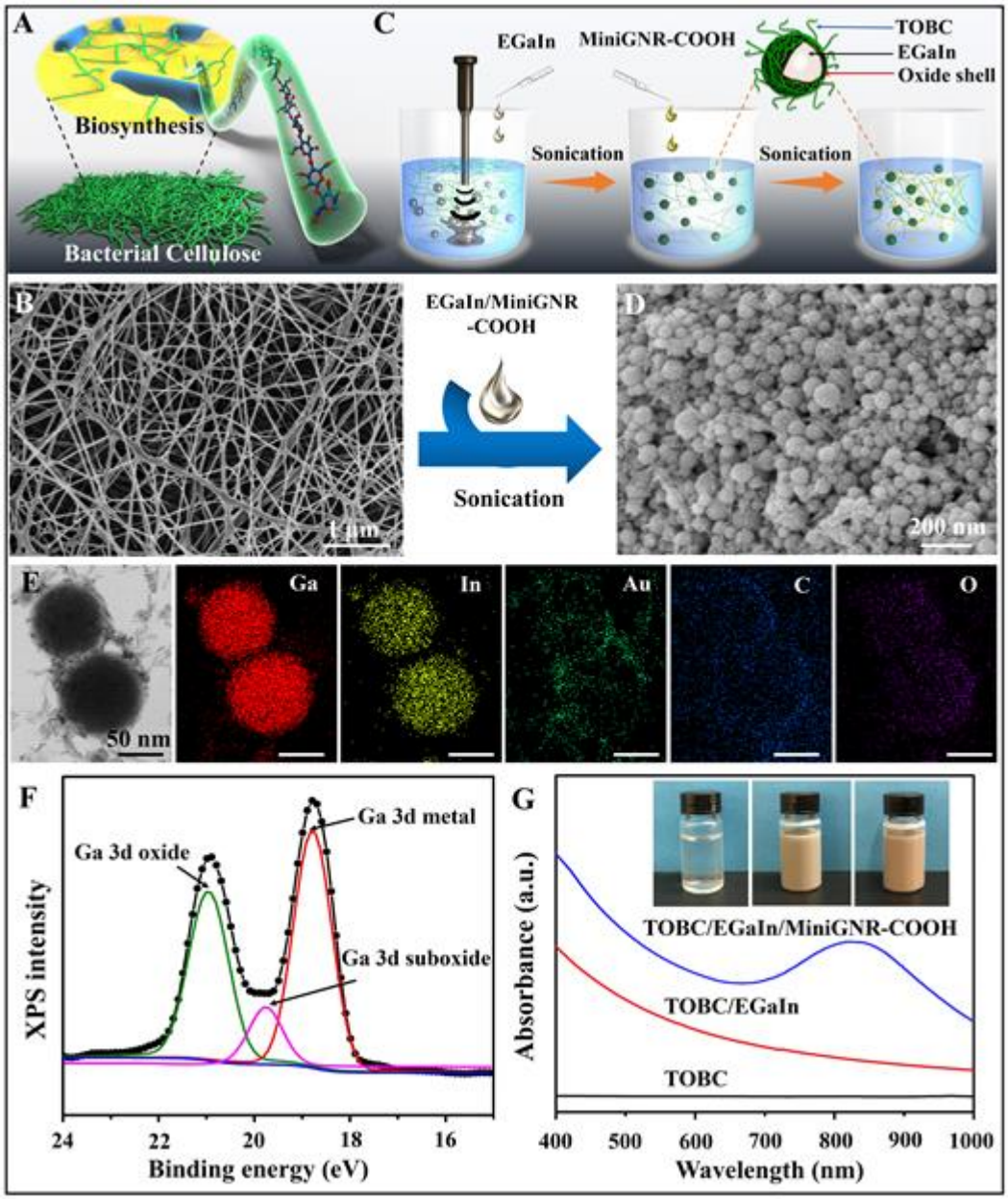

Fig. 1 Synthesis and characterizations of the colloidal LM ink. (A) Schematic biosynthesis of biological bacterial cellulose (BC), and (B) the corresponding SEM image of the BC nanofibers. (C) Schematic illustration of the fabrication of the colloidal LM ink by ultrasonicating bulk EGaIn LMs and MiniGNR-COOH in aqueous suspension of biological TOBC. (D) SEM image of the LM nanoparticles in the colloidal LM ink. (E) TEM image of the LM nanoparticles stabilized by TOBC and MiniGNR-COOH, and the corresponding elemental-mapping images (Ga, In, Au, C and O elements). (F) Ga 3d XPS profile of LM nanoparticles with characteristic peaks of Ga metal, Ga oxide and Ga suboxide. (G) UV-Vis spectra of TOBC, TOBC/EGaIn and TOBC/EGaIn/MiniGNR-COOH suspensions in deionized water. The insets show the corresponding images of TOBC (left), TOBC/EGaIn (middle) and TOBC/EGaIn/MiniGNR-COOH (right) suspensions.

advances have been achieved in the development of LM-based functional composites, it is still a formidable challenge to fabricate homogeneous LM composite systems with predictable and reliable performance because of the incompatibility between LMs and other materials. Therefore, robust soft-matter engineering strategies are urgently needed for effectively combining LMs and functional polymers or nanomaterials, while maintaining their excellent intrinsic properties, which in turn could facilitate the development of advanced multifunctional materials for untethered, programmable and reconfigurable soft robotics or machines with biomimetic intelligence.

Herein, we present a general strategy to develop shape-programmable LM-LCN soft actuators that combine the reversible shape-morphing properties of LCNs and superior thermal/electrical conductivity of LMs. A unique colloidal LM ink was judiciously designed and fabricated by ultrasonicating eutectic Gallium-Indium (EGaIn) LMs and miniature carboxylated gold nanorods (MiniGNR-COOH) in an aqueous suspension of biological nanocellulose. The

introduction of the MiniGNR-COOH is able to not only stabilize the LM nanoparticles, but also greatly enhance the photothermal properties of colloidal LM ink. The resulting colloidal LM ink could be facilely drop-casting deposited on a variety of substrates including shape-deformable LCN and SMP via evaporation-induced self-assembly. The as-prepared LM-LCN thin films exhibited excellent electrical conductivity and strong interfacial adhesion due to the evaporation-induced partially sintering of the LM microdroplets into a continuous conductive film in the presence of biological nanocellulose. Thus, the LM-LCN film could be electrothermally actuated using a low direct-current (DC) voltage. Near-infrared (NIR) light-driven LM-LCN soft actuators with robust shape-morphing and temporal programming features were achieved thanks to the superior photothermal conversion efficiency of embedded MiniGNR-COOH and selective coating characteristics of the colloidal LM inks. As proof-of-concept robotic functionalities, we developed a NIR light-fueled self-sustained soft oscillator under a constant NIR irradiation, and a light-driven inchworm-inspired soft crawler translocating on a ratcheted substrate through cyclic NIR irradiations. Moreover, we conceptualized NIR light-fueled programmable soft robotic Shadow Play, which is known as shadow puppets and an ancient form of storytelling and entertainment held between a source of light and a translucent screen, taking advantages of electrically conductive and shape-deformable LM-LCN and LM-SMP soft actuators. It is important to note that NIR light is particularly attractive for the realization of untethered soft robots thanks to its ubiquity, invisibility and spatiotemporal controllability.[41,42] The soft-matter engineering strategy disclosed herein is expected to pave a new avenue for efficiently combining the desired characteristics of LMs to those of functional polymers or nanomaterials, shining new light into the development of advanced multifunctional materials for untethered, programmable and reconfigurable soft robotics or machines with biomimetic intelligence.

Results and discussion

Fig. 1A schematically illustrates the biosynthesis of biological bacterial cellulose (BC). A type of aerobic bacterium, Komeigatabacter xylinum, was lab-cultured to produce BC pellicle at the air-liquid interface of the culture medium under static immersed cultivation conditions.[43,44] The resulting biodegradable BC films consist of three-dimensional interconnected network of cellulose nanofibers with high aspect ratio and an average diameter of ~ 30 nm (Fig. 1B and Fig. S1, ESI). Water-dispersed 2,2,6,6-tetramethylpiperidyl-1-oxyl (TEMPO)-oxidized bacterial cellulose (TOBC) nanofibers were prepared via an oxidation reaction with TEMPO radical. Successful oxidation of the hydroxyl groups was confirmed by monitoring the characteristic asymmetric C=O stretching vibration of carboxyl group, and the average diameter of TOBC nanofibers was decreased down to ~ 14 nm (Fig. S1, ESI).[45] The MiniGNR-COOH (~ 20 nm in length and ~ 5 nm in diameter) with superior photothermal properties that were much smaller than typical-sized gold nanorods with similar aspect ratio were synthesized by a hydroquinone-based seedless growth method (Fig. S2 and Fig. S3, ESI).[46] The colloidal LM ink was fabricated by ultrasonicating bulk EGaIn LMs and MiniGNR-COOH in the aqueous TOBC suspension, as shown schematically in Fig. 1C. To be more specific, 0.1 g of bulk EGaIn LM (78.6 wt% Ga and 21.4 wt% In, melting point ~ 15.8 °C) was firstly added into the aqueous TOBC suspension (20 mL, $Ø_{TOBC}$ = 0.2 wt%), and then ultrasonicated for 30 min in ice-bath water (TL-250Y, power of 650 W with 80% amplitude). 1 mL of MiniGNR-COOH aqueous solution ($Ø_{MiniGNR\text{-}COOH}$ = 0.4 wt%) was further added into the EGaIn/TOBC dispersion and the ultrasonication was performed for another 10 min in ice-bath water. Finally, size-grading was achieved by centrifuging at 4000 rpm. Further details about the synthetic process are given in the Supporting Information.

Scanning electron microscopy (SEM) and transmission electron microscopy (TEM) were implemented to characterize the nanostructures of the colloidal LM ink. As shown in Fig. 1D, the SEM image indicates the formation of stable and uniform spherical LM nanoparticles with an average size of ~ 70 nm due to the spontaneous oxidation on the surface under continuous ultrasonication and the coordination of Ga ions with the carboxyl groups of MiniGNR-COOH and TOBC. It was found that an optimal concentration of TOBC, 0.2 wt%, is critical to the formation of stable and uniform LM nanoparticles and the introduction of the MiniGNR-COOH could further stabilize the LM nanoparticles (Fig. S4 and Fig. S5, ESI). The energy-dispersive X-ray spectroscopy (EDX) in combination with SEM indicates the resulting nanostructured composites consist of 15.84 wt% (C), 7.23 wt% (O), 56.43 wt% (Ga), 12.33 wt% (In), and 8.17 wt% (Au) (Fig. S6, ESI). TEM image shows that LM nanoparticles are surrounded by TOBC nanofibers and MiniGNR-COOH (Fig. 1E and Fig. S7, ESI). Oxygen and carbon are clearly visible on the surface of the LM nanoparticles as evidenced by elemental-mapping images, and Au is homogeneously distributed throughout the individual nanofiber while concomitantly snuggling up to the surface of LM nanoparticles (Fig. 1E). X-ray photoelectron spectroscopy (XPS) shows the characteristic peaks at 18.7, 19.8 and 20.8 eV, which could be assigned to metallic gallium (Ga^0), gallium suboxide (Ga^{1+}) and gallium oxide (Ga^{3+}), respectively (Fig. 1F).[47] Interestingly, the resultant colloidal LM suspensions were stable for several days at pH ~ 7 under N_2 protection with negligible precipitation, which might be derived from their negatively charged surfaces (zeta potential: ~ -32 mV at pH 7) as well as the strong hydrogen bonding or Ga^{3+} coordination among LM nanoparticles, MiniGNRs-COOH and TOBC nanofibers (Fig. S8 and Fig. S9, ESI). The colloidal LM suspensions (TOBC/EGaIn/MiniGNR-COOH) exhibited a high optical absorption across visible and near infrared range (400-

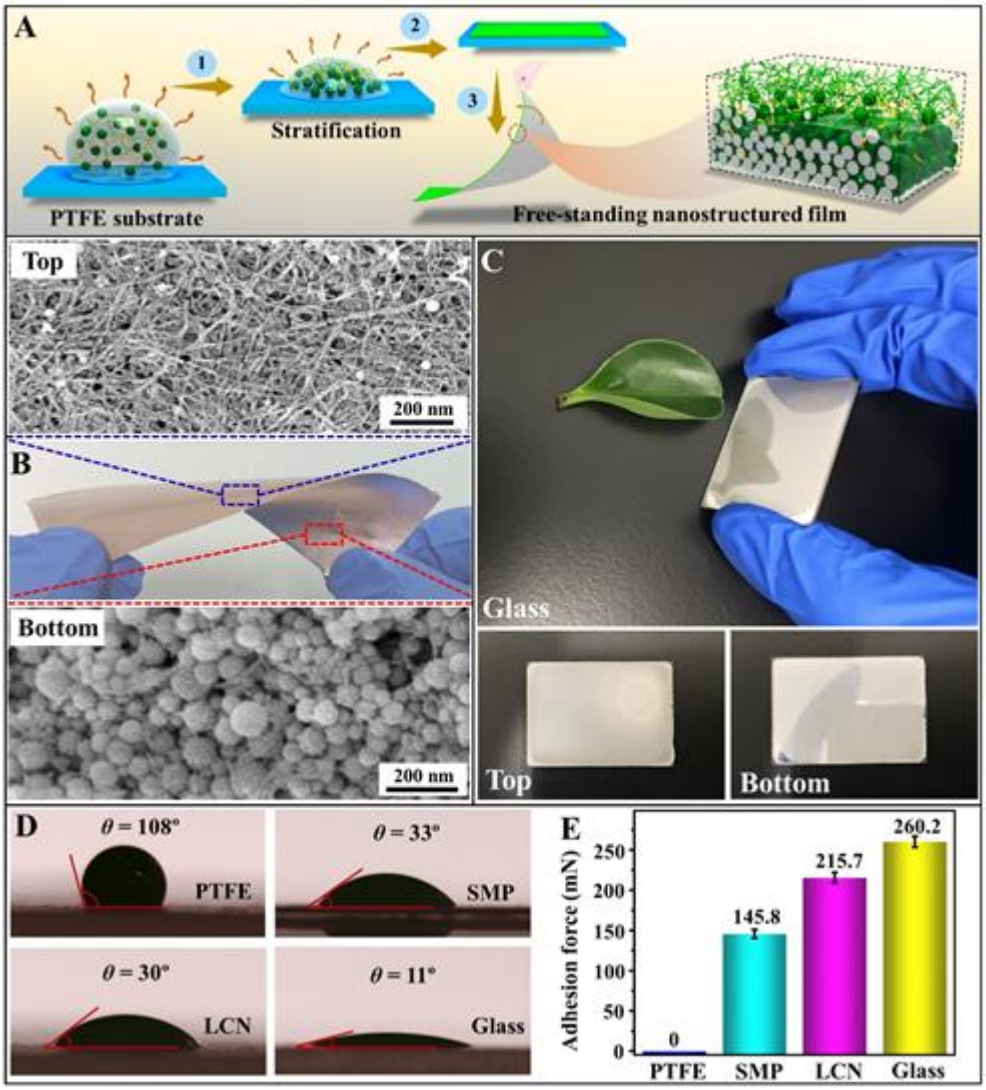

Fig. 2 Evaporation-induced self-assembly of the colloidal LM ink on different substrates. (A) Schematic self-assembly process of the colloidal LM ink on a PTFE substrate and evaporation-induced formation of free-standing nanostructured film. (B) Photograph of resultant free-standing nanostructured film (middle) and SEM images of its top and bottom surfaces. (C) Evaporation-induced deposition of the colloidal LM ink on transparent glass with grey top surface and mirror-like bottom surface. (D) The contact angles of the colloidal LM ink on PTFE, SMP, LCN and glass substrates. (E) Interfacial adhesion force of deposited colloidal LM coatings on PTFE, SMP, LCN and glass substrates.

1000 nm, Fig. 1G), and the absorption at 808 nm was significantly enhanced compared with the TOBC/EGaIn suspension due to the introduction of the MiniGNR-COOH. In the following experiments, 808 nm NIR light is applied for photoactuation thanks to the high photothermal conversion efficiency of the colloidal LM suspensions. The photothermal properties of the colloidal LM ink can be further enhanced upon increasing the concentration of MiniGNR-COOH (Fig. S10 and Fig. S11, ESI). It should be noted that the choice of irradiation wavelength is by no means limited and other wavelengths even sunlight can be used if desired.

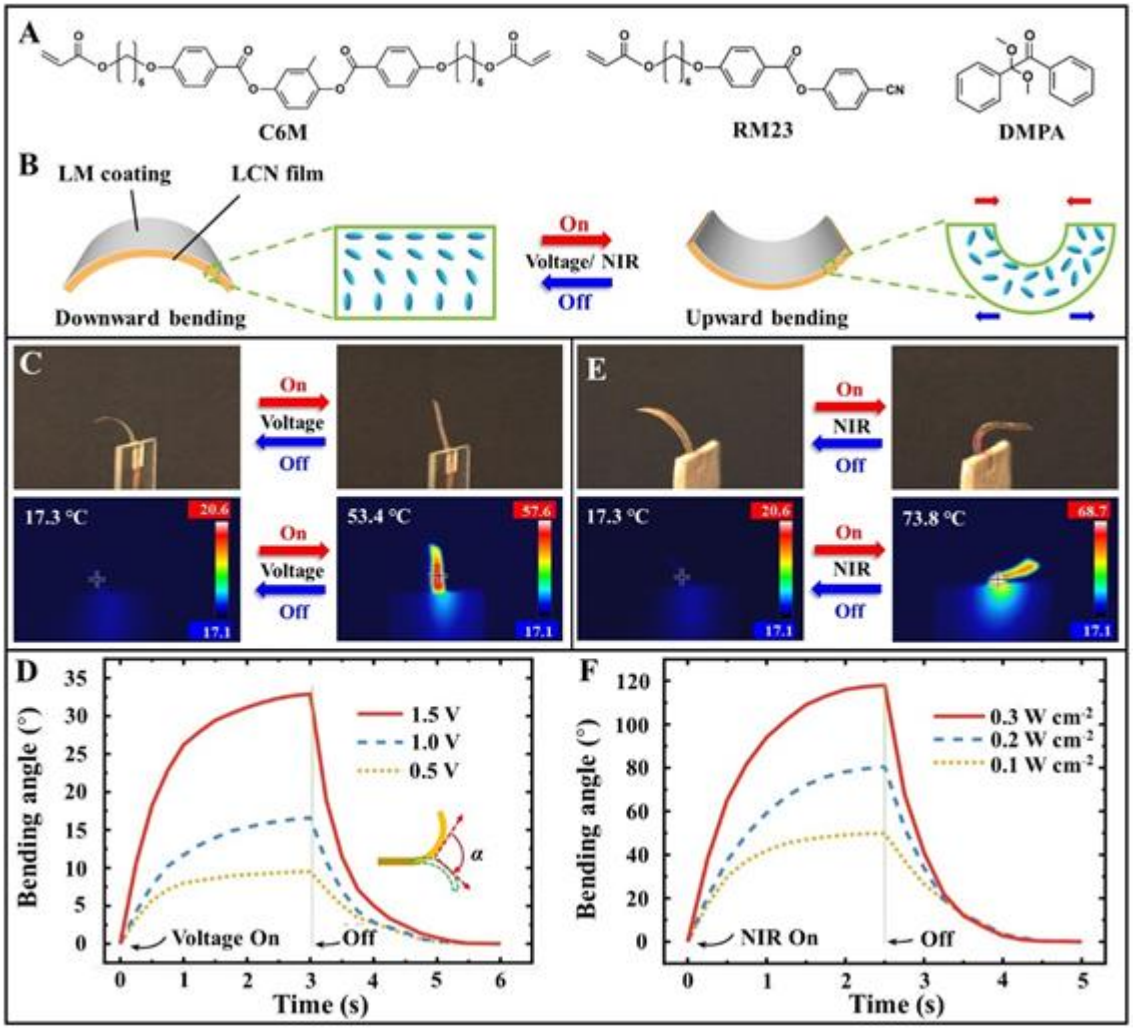

Fig. 3 Reversible shape deformation of the LM-LCN actuator upon applying DC voltage or NIR light irradiation. (A) Chemical structures of photopolymerizable liquid crystalline monomers (C6M and RM23) and photoinitiator (DMPA). (B) Schematics of the shape deformation of the LM-LCN hybrid film with splay molecular alignment. (C) Photographs and corresponding infrared thermal images showing the shape deformation of the LM-LCN under DC voltage. (D) The bending and unbending dynamics for different DC voltages (0.5 V, 1.0 V, and 1.5 V). (E) Photographs and corresponding infrared thermal images showing the shape deformation of the LM-LCN under NIR light irradiation (808 nm, 0.3 W cm^{-2}). (F) The bending and unbending dynamics for different light intensities (0.1 W cm^{-2}, 0.2 W cm^{-2}, and 0.3 W cm^{-2} at 808 nm).

To investigate the evaporation-induced self-assembly of the colloidal LM ink, the as-prepared colloidal LM suspension was deposited on different substrates by drop-casting followed by solvent evaporation and subsequent drying process at the ambient conditions (1 atm, ~ 25 °C, ~ 40 RH%). Fig. 2A shows the schematic evaporation-induced self-assembly process of the colloidal LM ink on a polytetrafluoroethylene (PTFE) substrate. After solvent evaporation, we obtained a free-standing nanostructured thin film that was automatically detached from the PTFE substrate, as shown in Fig. 2B. SEM images indicate the presence of TOBC nanofibers on the top surface and the formation of stacked LM nanoparticles on the bottom surface. The cross-sectional TEM and EDX elemental-mapping images further confirmed the gradient in LM nanoparticle distribution across the thickness of the nanostructured film, while the MiniGNR-COOH were homogeneously distributed throughout the whole film (Fig. S12 and Fig. S13, ESI). Meanwhile, the resultant nanostructured thin film exhibited satisfactorily electrical conductivity (3.2×10^5 S m^{-1}) and could serve as a conductive layer for flexible electronics, which might result from the evaporation-induced deposition of LM nanoparticles in the presence of bacterial cellulose (Fig. S15, ESI). It should be noted that the introduction of the MiniGNR-COOH was able to enhance the photothermal, electrical and mechanical properties of the free-standing nanostructured thin film (Fig. S14, Fig. S15 and Fig. S16, ESI). Interestingly, grey top surface and mirror-like bottom surface were observed upon evaporation-induced deposition of the colloidal LM

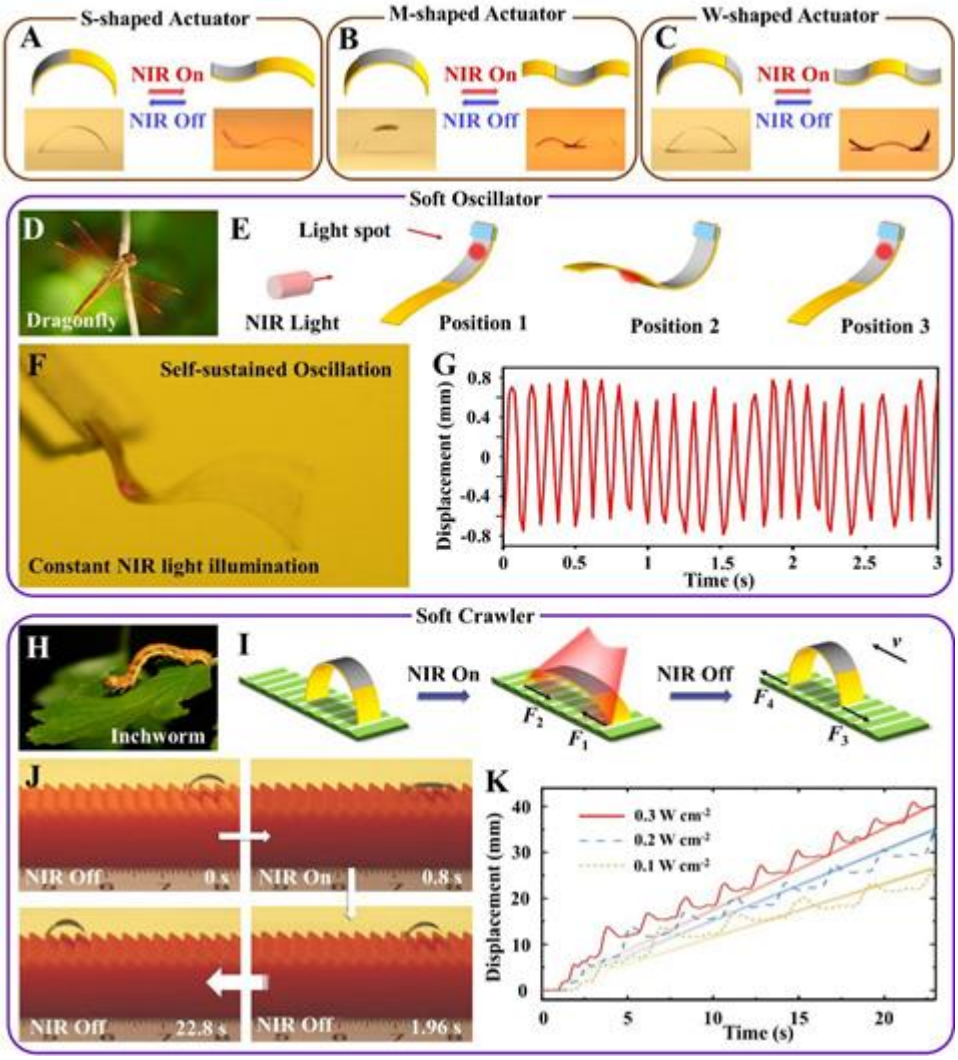

Fig. 4 NIR light-driven shape-programmable LM-LCN soft actuators. (A) Half-patterning (Width = 4 mm, Length = 15 mm), (B) center-patterning (Width = 4 mm, Length = 6 mm) and (C) edge-patterning (Width = 4 mm, 5 mm spacing, Length = 6 mm) of colloidal LM ink on the LCN film and light-driven shape-morphing upon NIR irradiation. (D) A dragonfly in nature. (E) Schematic illustration of light-driven self-sustained soft oscillator made of half-patterned LM-LCN actuator under constant NIR irradiation. (F) Overlay of frames visualizing self-sustained oscillation. (G) The displacement of the LM-LCN actuator during the self-oscillation process. (H) An inchworm in nature. (I) Schematic illustration and (J) real images of light-driven inchworm-inspired soft crawler made of center-patterned LM-LCN actuator translocating on a ratcheted substrate upon cyclic NIR irradiations. (K) The crawling distance and speed upon cyclic NIR irradiations under different light intensities (0.1 W cm^{-2}, 0.2 W cm^{-2}, and 0.3 W cm^{-2} at 808 nm).

suspension on a transparent glass substrate (Fig. 2C). Furthermore, the colloidal LM coating exhibited excellent adhesion and was difficult to peel off from some substrates such as glass, SMP and LCN (Fig. S17, ESI). Fig. 2D illustrates the contact angles of the colloidal LM ink on different substrates. Maximum value of 108° was observed on PTFE, being substantially lower on SMP, LCN and glass, 33°, 30° and 11°, respectively. Fig. 2E shows the interfacial adhesion force of the deposited colloidal LM coatings on these substrates, indicating that a decrease in the contact angle is beneficial for enhancing the interfacial adhesion strength. The superior interfacial adhesion properties of the LM coatings on SMP and LCN substrates make it possible to efficiently combine LMs and functional polymer materials, setting the basis for the LM-based soft actuators that follow.

Shape-deformable LM-LCN soft actuators were fabricated through drop-casting of the colloidal LM suspension onto the LCN film with the mesogenic molecules aligned in a splay configuration. Flexible LCN films with a thickness of ~ 23 μm were prepared by photopolymerization of liquid crystalline monomers (C6M:RM23 = 70:30 wt%, 0.5 wt% photoinitiator DMPA) as shown in Fig. 3A under UV irradiation (365 nm, 10 mW cm^{-2}) at the temperature of ~ 70 °C. The obtained splay-aligned LCN film shows an initial curvature due to the anisotropic thermal expansion during cooling from polymerization temperature to room temperature. The LM coating with a thickness of 0.3 μm was developed through drop-casting deposition of colloidal LM suspension on the planar side of LCN film followed by solvent evaporation and subsequent drying at the ambient condition (Fig. S18, ESI). As illustrated in Fig. 3B, the splay molecular alignment enabled a gradual change in the director of the LC molecules from planar to homeotropic through the thickness of the LCN film. Thanks to the superior interfacial adhesion properties of the colloidal LM coating, the obtained LM-LCN soft actuator exhibited reversible shape deformation upon applying DC electric

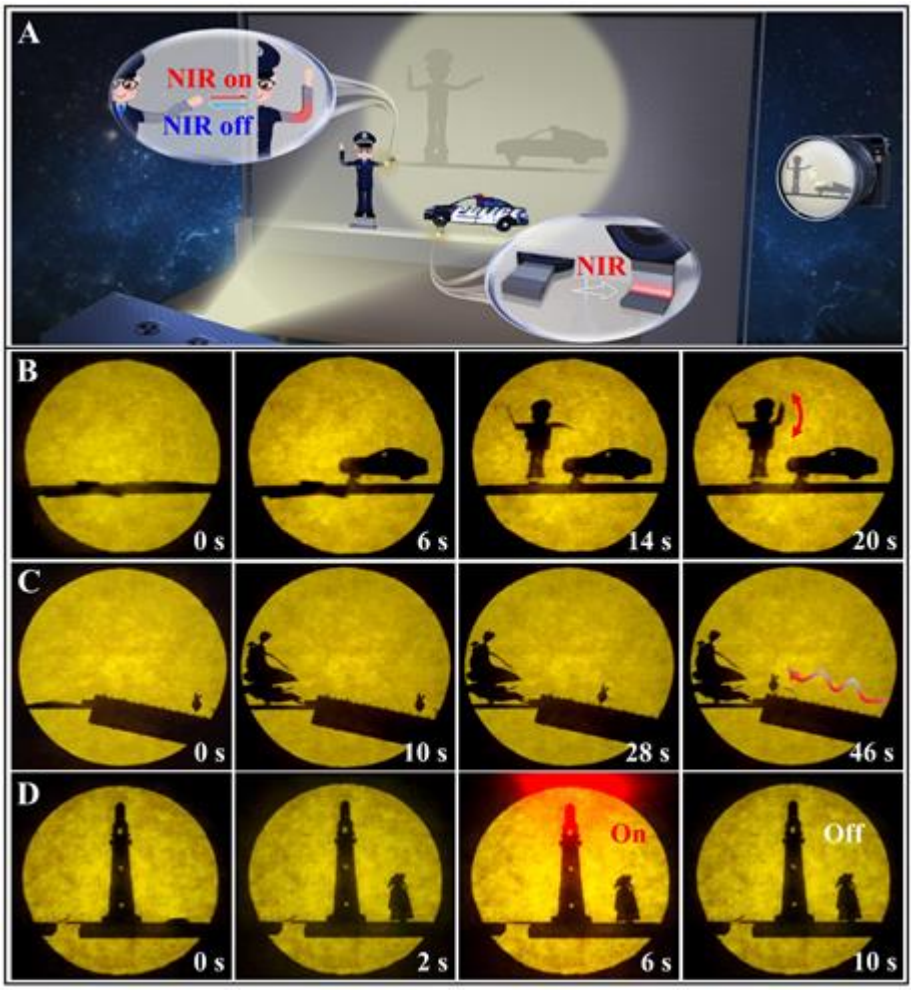

Fig. 5 NIR light-fueled programmable soft robotic Shadow Play through the integration of shape-deformable LM-LCN and shape-memory LM-SMP soft actuators. (A) Schematic illustration of robotic shadow puppets located between a white light source and a translucent screen. Images of light-driven Shadow Play with different robotic functions upon NIR irradiation (808 nm, 0.2 W cm^{-2}): (B) A police officer directing the traffic; (C) A Jade Rabbit walking toward the Beauty; (D) A person looking up at the shining beacon.

field or NIR light irradiation, which could be attributed to the electrothermally and photothermally induced decrease in liquid crystalline ordering and the resulting contraction at the planar side and expansion at the homeotropic side of the film.[48] Fig. 3C indicates that the LM-LCN film could be electrothermally actuated through applying a low DC voltage thanks to the excellent electrical conductivity of the colloidal LM coating layer and the resultant electrothermal Joule-heating, as clearly observed in the corresponding infrared thermal images. The maximum shape-bending angle of the actuator can be controlled by the applied voltage, reaching 34° within 3.0 s under 1.5 V, and restoration of the initial shape within 2 s upon switching off the voltage (Fig. 3D, Fig. S19 and S20, ESI). Fig. 3E illustrates the photoinduced shape-deformation behavior of LM-LCN actuator under NIR light irradiation (808 nm, 0.3 W cm^{-2}). The corresponding infrared thermal image indicates the superior photothermal conversion efficiency under NIR light irradiation. The bending angle of the LM-LCN actuator was dependent on the intensity and time of NIR irradiation, restoring back to the initial state when ceasing the light (Fig. 3F). When the light intensity is 0.3 W cm^{-2}, the actuator reached a bending angle of 118° within 2.5 s. The reversible shape-deformation of the LM-LCN actuator could be repeatedly for over 100 cycles without any noticeable degradation, indicating excellent reversibility in actuation (Fig. S21, ESI). It was found that the actuation performance of LM-LCN soft actuator could be greatly enhanced with an increasing thickness of LM coatings on 23.0 μm-thick LCN film, which might be attributed to an increasing content of LM and MiniGNR-COOH, and subsequent enhanced photothermal effect. However, when the thickness of LM coating increases to a certain extent such as 5 μm, the LM-LCN soft actuator exhibits a decreased actuation performance, where a large thickness of the LM coating could restrict the shape-deformation of LCN layer (Fig. S22 and S23, ESI). With a constant thickness of LM coating (0.3 μm), the bending angle of LM-LCN soft actuator decreases upon increasing the thickness of the LCN film from 23 μm to 69 μm (Fig. S24 and S25, ESI). Therefore, photoresponsive dynamics of LM-LCN soft actuators are closely related to several factors such as the thickness of LCN film, thickness of colloidal LM coating and power density of NIR irradiations.

NIR light-driven LM-LCN actuators with programmable shape-morphing were developed by drop-casting the colloidal LM ink on selected areas of the planar side of the splay-aligned LCN films. The LCN films exhibit an initial curvature due to the anisotropic thermal

expansion during the cooling process from polymerization temperature to room temperature. When the nanostructured colloidal LM coating was only deposited onto one half of the LCN film (Fig. 4A), a reversible S-shaped actuation was obtained under the NIR light irradiation (Movie S1). M- and W-shaped actuators could be achieved by applying the same colloidal LM coating onto the middle part and the two ends of the LCN film, respectively (Fig. 4B, Fig. 4C and Movie S1, ESI). Taking inspiration from the oscillation phenomena in nature such as dragonflies' wings (Fig. 4D), we conceptualized a NIR light-fueled LM-LCN self-sustained soft oscillator with a frequency of ~ 8.0 Hz, where a steady and sustainable oscillation motion of the cantilever with colloidal LM coating deposited onto one half of the LCN film was observed under a constant NIR light illumination (Movie S2, 808 nm and 0.2 W cm^{-2}, ESI). Fig. 4E schematically illustrates the self-shadowing mechanism of such self-sustained oscillation: Initially, the LCN region with colloidal LM coating was exposed to NIR light (Position 1), resulting in photothermal heating of the LCN film and bending deformation towards the light source until the colloidal LM-coated region was shadowed by the blank edge (Position 2). Consequently, the temperature of the colloidal LM-coated region decreased and the film shape was recovered (Position 3), re-exposing the colloidal LM-coated region again (Position 1) and starting a new oscillation cycle.[49,50] Governed by self-shadowing, the cantilever could self-oscillate under constant NIR irradiation with frequency of 8.0 $\pm$ 0.5 Hz (Fig. 4F and 4G). We further demonstrated a light-driven inchworm-inspired soft robotic crawler made of center-patterned LM-LCN translocating on a ratcheted substrate. The robot was excited upon cyclic NIR irradiations as shown in Fig. 4H-4J and Movie S3 (ESI). The LM-LCN actuator underwent downward shape-bending on the surface of the ratcheted substrate under NIR irradiation, where the back edge bearing larger frictional force (F1 > F2) acts as a stationary end and thus the downward bending leads to forward movement of the front part of the crawler. Upon ceasing the light, unbending occurs due to elastic recovery of the LCN strip, and the front edge bears larger frictional force (F4 > F3) acting as a stationary end to allow for the crawler to move its back part forward, thus leading to inchworm-like translocation along the ratcheted substrate.[51] The crawling kinetics of the LM-LCN actuator under different NIR intensities is presented in Fig. 4K. The mean speed was found to be 1.17, 1.51, and 1.75 mm s^{-1} for 0.1, 0.2, and 0.3 W cm^{-2} light intensities at 808 nm. Taking advantage of the high photothermal conversion efficiency, superior interfacial adhesion and programmable coating properties of colloidal LM suspensions, we also demonstrated self-folding of 2D shape memory polymer (SMP) sheets with predesignated colloidal LM coatings into various 3D objects under the exposure of NIR light, and temporal programming of shape morphing and sequential self-folding were easily achieved by tailoring the thickness of the designed colloidal LM hinges (Fig. S26 and Movie S4, ESI).

Lastly, we realize complex robotic Shadow Plays by assembling LM-based responsive soft actuator building blocks with spatiotemporal controllability and multiple functionalities. Shadow Play is an ancient form of storytelling and entertainment in many countries around the world, where shadow puppets in the form of diverse flat articulated cut-out figures are held between a source of light and a translucent screen.[52] The shadows cast against the screen are used to express a story through manually manipulating the puppets' diverse motions. Here, a programmable robotic Shadow Play was demonstrated through the integration of LM-SMP with shape-memory behavior and electrically conductive shape-deformable LM-LCN actuators. The Shadow Play was controlled by light, as schematically shown in Fig. 5A, where a puppet (police officer) directs the traffic and the motion is projected onto a screen observed by the audience (camera). As shown in Fig. 5B and Movie S5 (ESI), the shadow of the robotic puppets was absent at the beginning since the puppets made of shape reversible LM-LCN (hand) and shape irreversible LM-SMP (body) actuators were kept at horizontal state invisible to the screen. Shining NIR light on the car's front wheel, the photothermally induced irreversible deformation of the LM-SMP hinge led to the appearance of the car's shadow on the screen, i.e., the cut-out figure of the car stood up on the support. Similarly, NIR irradiation of the policeman's foot and hand with LM-SMP hinges resulted in the shadow of the policeman with one hand raised up appearing on the screen. The policeman's other hand with LM-LCN actuator as elbow joint could exhibit reversible hand-waving gestures through cyclic light irradiations. The second robotic Shadow Play is inspired by the Chinese legends of the Beauty Chang'e flying to the moon, and Fig. 5C shows the scene of a Jade Rabbit walking toward the Beauty. Synchronization of the NIR light excitation and robotic shadows is shown in Movie S6 (ESI). Upon NIR irradiation, the photothermally induced irreversible deformation of LM-SMP hinge on the Beauty's foot led to her appearance. Light-driven Jade Rabbit's walking up to the Beauty is triggered by LM-LCN actuator translocating on a ratcheted sky ladder upon cyclic NIR irradiation. Fig. 5D and Movie S7 (ESI) demonstrate the scene of a person looking up at the shining beacon based on the LM-LCN and LM-SMP soft actuators as well as electrical conductivity of colloidal LM coating layers. The beacon with light off was presented on the translucent screen at the beginning, and NIR irradiations of the person's foot equipped with LM-SMP hinge led to the shadow of the person standing and looking up the lit beacon appearing. The red LED on the top of the beacon could be reversibly switched through NIR light-driven bending deformation of electrically conductive LM-LCN film connected to/disconnected from an electric circuit.

Conclusion

In this work, we have demonstrated shape-programmable LM-LCN soft actuators that combine reversible shape-morphing properties of LCNs and superior electrical conductivity of LMs. A colloidal LM ink with high stability and enhanced photothermal effects via the MiniGNR-COOH incorporations was developed. The introduction of the MiniGNR-COOH is able to not only stabilize the LM nanoparticles, but also enhance the photothermal properties of colloidal LM ink. The resulting colloidal LM ink could be facilely deposited on a variety of substrates such as PTFE, SMPs, LCNs and glass through a simple drop-casting technique. The resultant nanostructured thin coatings or films exhibited high electrical conductivity and interfacial

adhesion due to evaporation-induced partially sintering of the LM microdroplets into a continuous conductive film in the presence of biological nanocellulose. Electrothermally and photothermally driven shape-morphing LM-LCN soft actuators were developed through drop-casting of the colloidal LM ink onto splay-aligned LCN film. The LM-LCN soft actuators could be electrothermally actuated upon applying a low DC voltage due to the excellent electrical conductivity of the colloidal LM coating layer. NIR light-driven shape-programmable LM-LCN soft actuators with diverse shape deformations were fabricated by selectively drop-casting the colloidal LM ink on the planar side of splay-aligned LCN films. As the proof-of-concept robotic applications, NIR light-fueled self-sustained soft oscillator with oscillation frequency of ~ 8.0 Hz and light-driven inchworm-inspired soft crawler were demonstrated. Moreover, we presented a NIR light-driven programmable robotic Shadow Play through the integration of shape-deformable LM-LCN and shape-memory LM-SMP soft actuators. Compared with the other most relevant comparable systems (Table S1, ESI), herein we demonstrate a more general strategy to efficiently integrate electrically conductivity of LMs and shape-morphing properties of LCNs or functional polymers while maintaining their excellent intrinsic properties. The results disclosed here could provide new impetus toward the development of untethered soft robotics or machines with biomimetic intelligence, integrated multifunctional flexible electronics, human-computer interaction as well as other advanced biomedical technologies.

Conflicts of interest

The authors have no conflicts of interest to declare.

Acknowledgements

This work was financially supported by National Natural Science Foundation of China (No. 51973155 and 52003191), National Key R&D Program of China (No. 2016YFA0202302), State Key Program of National Natural Science Foundation of China (No. 51633007), Postdoctoral Science Foundation of China (No. 2019M661015), and Academy of Finland (Flagship Programme PREIN, No. 320165 and a postdoctoral grant No. 326445).

References

1. M. P. D. Cunha, M. G. Debije and A. P. H. J. Schenning, *Chem. Soc. Rev.*, 2020, **49**, 6568-6578.
2. H. Zhang, H. Zeng, A. Priimagi and O. Ikkala, *Adv. Mater.*, 2020, **32**, 1906619.
3. Q. Li (Ed.), Intelligent stimuli responsive materials: from well-defined nanostructures to applications (John Wiley & Sons, Hoboken, NJ, 2013).
4. F. Lancia, A. Ryabchun and N. Katsonis, *Nat. Rev. Chem.*, 2019, **3**, 536-551.
5. D. Rus and M. T. Tolley, *Nature*, 2015, **521**, 467-475.
6. L. Hines, K. Petersen, G. Lum and M. Sitti, *Adv. Mater.*, 2017, **29**, 1603483.
7. J. M. McCracken, B. R. Donovan and T. J. White, *Adv. Mater.*, 2020, **32**, 1906564.
8. J. Liu, Y. Gao, Y. J. Lee and S. Yang, *Trends in Chem.*, 2020, **2**, 107-122.
9. S. J. Jeon, A. W. Hauser and R. C. Hayward, *Acc. Chem. Res.*, 2017, **50**, 161-169.
10. L. Tang, L. Wang, X. Yang, Y. Y. Feng and W. Feng, *Prog. Mater. Sci.*, 2021, **115**, 100702.
11. P. Xue, H. K. Bisoyi, Y. Chen, H. Zeng, J. Yang, X. Yang, P. Lv, X. Zhang, A. Priimagi, L. Wang, X. Xu and Q. Li, *Angew. Chem. Int. Ed.*, 2020, DOI: 10.1002/anie.202014533.
12. Y. Chen, J. Yang, X. Zhang, Y. Feng, H. Zeng, L. Wang and W. Feng, *Mater. Horiz.*, 2020, DOI: 10.1039/D0MH01406K.
13. C. Majidi, *Adv. Mater. Technol.*, 2019, **4**, 1800477.
14. T. J. White and D. J. Broer, *Nat. Mater.*, 2015, **14**, 1087-1098.
15. J. Lv, Y. Liu, J. Wei, E. Chen, L. Qin and Y. Yu, *Nature*, 2016, **537**, 179-184.
16. H. Shahsavan, A. Aghakhani, H. Zeng, Y. Guo, Z. S. Davidson, A. Priimagi and M. Sitti, *Proc. Natl. Acad. Sci. U.S.A.*, 2020, **117**, 5125-5133.
17. H. Zeng, W. Piotr, D. S. Wiersma and A. Priimagi, *Adv. Mater.*, 2018, **30**, 1870174.
18. H. Zeng, O. M. Wani, P. Wasylczyk, R. Kaczmarek and A. Priimagi, *Adv. Mater.*, 2017, **29**, 1701814.
19. M. Lahikainen, H. Zeng and A. Priimagi, *Nat. Commun.*, 2018, **9**, 4148.
20. Q. He, Z. Wang, Y. Wang, A. Minori, M. T. Tolley and S. Cai, *Sci. Adv.*, 2019, **5**, eaax5746.
21. H. Zeng, H. Zhang, O. Ikkala and A. Priimagi, *Matter*, 2020, **2**, 194-206.
22. Y. Wang, A. Dang, Z. Zhang, R. Yin, Y. Gao, L. Feng and S. Yang, *Adv. Mater.*, 2020, **32**, 202004270.
23. H. Yu and T. Ikeda, *Adv. Mater.*, 2011, **23**, 2149-2480.
24. H. K. Bisoyi and Q. Li, *Chem. Rev.*, 2016, **116**, 15089-15166.
25. X. Wang, R. Guo and J. Liu, *Adv. Mater. Technol.*, 2019, **4**, 1800549.
26. J. Liu, L. Sheng and Z. He, Liquid metal soft machines: principles and applications (Springer, 2018).
27. S. Chen, H. Z. Wang, R. Q. Zhao, W. Rao and J. Liu, *Matter*, 2020, **2**, 1446-1480.
28. M. H. Malakooti, M. R. Bockstaller, K. Matyjaszewski and C. Majidi, *Nanoscale Adv.*, 2020, **2**, 2668-2677.
29. Y. Lu, Y. Lin, Z. Chen, Q. Hu, Y. Liu, S. Yu, W. Gao, M. D. Dickey and Z. Gu, *Nano Lett.*, 2017, **17**, 2138.
30. T. Gan, W. Shang, S. Handschuh-Wang and X. Zhou, *Small*, 2019, **15**, 1804838.
31. S. A. Chechetka, Y. Yu, X. Zhen, M. Pramanik, K. Pu and E. Miyako, *Nat. Commun.*, 2017, **8**, 15432.
32. C. Pan, E. J. Markvicka, M. H. Malakooti, J. Yan, L. Hu, K. Matyjaszewski and C. Majidi, *Adv. Mater.*, 2019, **31**, 1900663.

33. M. D. Bartlett, N. Kazem, M. J. Powell-Palm, X. Huang, W. Sun, J. A. Malen and C. Majidi, *Proc. Natl. Acad. Sci. U.S.A.*, 2017, 114, 2143-2148.
34. E. J. Markvicka, M. D. Bartlett, X. Huang and C. Majidi, *Nat. Mater.*, 2018, **17**, 618.
35. M. J. Ford, D. K. Patel, C. Pan, S. Bergbreiter and C. Majidi, *Adv. Mater.*, 2020, **32**, 2002929.
36. X. Li, M. Li, J. Xu, J. You, Z. Yang and C. Li, *Nat. Commun.*, 2019, **10**, 3514.
37. P. Zhang, Q. Wang, R. Guo, M. Zhang, S. Wang, C. Lu, M. Xue, J. Fan, Z. He and W. Rao, *Mater. Horiz.*, 2019, **6**, 1643.
38. M. J. Ford, C. P. Ambulo, T. A. Kent, E. J. Markvicka, C. Pan, J. Malen, T. H. Ware and C. Majidi, *Proc. Natl. Acad. Sci. U.S.A.*, 2019, **116**, 21438.
39. C. P. Ambulo, M. J. Ford, K. Searles, C. Majidi and T. H. Ware, *ACS Appl. Mater. Interfaces*, 2021, DOI: 10.1021/acsami.0c19051.
40. S. Veerapandian, W. Jang, J. B. Seol, H. Wang, M. Kong, K. Thiyagarajan, J. Kwak, G. Park, G. Lee, W. Suh and I. You, *Nat. Mater.*, 2021, DOI: 10.1038/s41563-020-00863-7.
41. L. Wang, H. Dong, Y. Li, R. Liu, Y. Wang, H. K. Bisoyi, L. D. Sun, C. H. Yan and Q. Li, *Adv. Mater.*, 2015, **27**, 2065-2069.
42. L. Wang and Q. Li, *Chem. Soc. Rev.*, 2017, **47**, 1044-1079.
43. D. Klemm, F. Kramer, S. Moritz, T. Lindström, M. Ankerfors, D. Gray and A. Dorris, *Angew. Chem. Int. Ed.*, 2011, **50**, 5438-5466.
44. P. Lv, H. Zhou, A. Mensah, Q. Feng, D. Wang, X. Hu, Y. Cai, L. A. Lucia, D. Li and Q. Wei, *Chem. Eng. J.*, 2018, **351**, 177-188.
45. S. S. Kim, J. H. Jeon, H. I. Kim, C. D. Kee and I. K. Oh, *Adv. Funct. Mater.*, 2015, **25**, 3560-3570.
46. Y. S. Chen, Y. Zhao, S. J. Yoon, S. S. Gambhir and S. Emelianov, *Nat. Nanotech.*, 2019, **14**, 465-472.
47. A. Yamaguchi, Y. Mashima and T. Iyoda, *Angew. Chem. Int. Ed.*, 2015, **54**, 12809-12813.
48. R. Lan, J. Sun, C. Shen, R. Huang, Z. Zhang, L. Zhang, L. Wang and H. Yang, *Adv. Mater.*, 2020, **32**, 1906319.
49. A. H. Gelebart, D. J. Mulder, M. Varga, A. Konya, G. Vantomme, E. W. Meijer, R. L. Selinger and D. J. Broer, *Nature*, 2017, **546**, 632-636.
50. A. H. Gelebart, G. Vantomme, E. W. Meijer and D. J. Broer, *Adv. Mater.*, 2017, **29**, 1606712.
51. X. Lu, H. Zhang, G. Fei, B. Yu, X. Tong, H. Xia and Y. Zhao, *Adv. Mater.*, 2018, **30**, 1706597.
52. D. Currell, Shadow puppets and shadow play (Crowood Press, 2015).

Table of Contents

Shape-programmable soft actuators are developed through an integration of electrically conductive liquid metals with shape-morphing liquid crystal networks. The proof-of-concept robotic functionalities including light-fueled soft oscillator, inchworm-inspired soft crawler and programmable robotic Shadow Play are demonstrated.